

# Compact binaries detection rates from gravitational wave interferometers: comparison of different procedures

G. Corvino,<sup>1,\*</sup> V. Ferrari,<sup>1</sup> S. Marassi,<sup>1</sup> and R. Schneider<sup>2</sup>

<sup>1</sup>*Dipartimento di Fisica ‘G. Marconi’, Sapienza Università di Roma  
and Sezione INFN Roma1, Piazzale Aldo Moro 5, Roma, 00185, Italy*

<sup>2</sup>*INAF, Osservatorio Astronomico di Roma, via di Frascati 33, 00040 Monteporzio Catone, Italy*

(Dated: March 21, 2022)

In this paper we perform a detailed analysis of the effect of various approximations which have been used in the literature to compute the detection rates of compact binary coalescences for interferometric gravitational wave detectors. We evaluate the detection rates for the coalescence of BH-BH, NS-NS, and BH-NS binaries taking into account their specific statistical properties obtained from population synthesis models, the cosmic star formation rate history, and the effects of redshift on the emitted gravitational wave signals. The results are compared with those obtained with procedures that are based on different levels of approximations, such as adopting averaged values for the total mass and symmetric mass ratio for all the systems of a binary population, using these to compute the horizon distance for individual detectors, or estimating the coalescence rate density within this distance by its local value. We show that these approximations introduce a bias which depends not only on the approximation which is used, but also on the statistical properties of the considered binary population.

PACS numbers: to be inserted

## I. INTRODUCTION

The second generation of gravitational wave interferometers, Advanced Virgo<sup>1</sup> and LIGO<sup>2</sup>, will push ten times farther their observational reach, opening a much wider region of the Universe to observations. Furthermore, the third-generation ground-based observatory Einstein Telescope (ET)<sup>3</sup>, which is currently in a design study phase, is expected to improve the sensitivity by a further factor of ten [1, 2]. This will allow to detect gravitational wave (GW) signals emitted by astrophysical sources, for instance the coalescence of compact binaries in which we are primarily interested, with sufficiently high signal-to-noise ratios (SNR) and rates, to allow precise astronomical studies of these sources [3]. In addition, the high sensitivity of these detectors will allow to see beyond our local universe, accessing regions of redshift where the role of the star formation history and of cosmological models becomes important, and could be tested ([4–6] and references therein).

The detection of a GW signal is based on the correlation of the output data stream of the detector with an expected signal, which is typically in the form of a template. Given the high number of parameters needed to model a source, a complete survey of the parameter space is often impossible. For this reason it is important to know what are the systems that are more likely to be detected and their expected properties [7, 8]. In recent

years several papers have been published where the coalescence rates of compact binaries, and the corresponding detection rates by GW detectors, have been estimated by using several approximations [9–22].

In this paper we study in detail the effects of these approximations on the detection rates of advanced detectors, also showing to what extent these effects depend on the binary population model which is used. We choose, as an example, two models generated by the code **Startrack**, and publicly available<sup>4</sup>. Details on the physical inputs of the simulation are given in [23]. The binary populations are the result of the evolution of a large sample ( $N = 2 \cdot 10^6$ ) of “zero-age” binaries.

Using these data, we compute the coalescence and detection rates of binaries composed of two black holes, BH-BH, two neutron stars, NS-NS, a black hole and a neutron star, BH-NS, using a completely consistent procedure based on the appropriate use of the statistical properties of the populations, and on the redshift dependence of the star formation rate history [10, 11, 24, 25]. The detection rates are given for Advanced Virgo and LIGO, and for ET.

These rates are then compared with those computed by applying, to the same populations, the different approximations used in the literature, to evaluate the bias they introduce (if any), to show how this varies for the Advanced detectors in different configurations, and to understand its dependence on the population properties.

The statistical properties of coalescing binary populations depend on the physical inputs of the population synthesis codes, which may vary significantly from one

---

\*Electronic address: giovanni.corvino@roma1.infn.it

<sup>1</sup> <https://www.cascina.virgo.infn.it/advirgo/>

<sup>2</sup> <http://www.ego-gw.it/>, <http://www.ligo.caltech.edu>

<sup>3</sup> ET: [www.et-gw.eu](http://www.et-gw.eu)

---

<sup>4</sup> <http://www.syntheticuniverse.org>

model to another. The choice of the two models we consider in this paper, together with their main statistical properties, are briefly described in section II.

We will show that in order to obtain detection rate estimates which depend only on the properties of the binary population, we need to use a fully consistent approach, since each of the approximations used in the literature leads to over/underestimate these rates by amounts which depend on the population properties.

The plan of the paper is the following. In section II we describe the fully consistent procedure to compute the coalescence and detection rates for a simulated population of compact binaries. In section III we describe various approximations used to evaluate the rates [9, 20, 21], apply them to the two population models we consider, and compare the results with those found with no approximation. Concluding remarks are given in section IV.

## II. RATE COMPUTATION PROCEDURE

The binary population models we use to compute coalescence and detection rates, are chosen from the Standard model of [23], since this model is the fiducial one, being based on conservative assumptions. We consider the two submodels A which correspond to progenitor stars with solar and subsolar metallicity. The corresponding populations exhibit different mass distributions, and this is the feature which is of major interest for us. Hereafter we will refer to these two models as model A (solar metallicity) and model B (subsolar metallicity).

Here we report some statistical properties of each model, which will be useful in the following to understand the results. First of all, it should be mentioned that, as a result of different physical inputs (which we do not discuss here), the number of binaries coalescing within the Hubble time, differs in the two models: for model A there are 1753 BH-BH binaries, 5084 NS-NS and 345 BH-NS; for model B the population is made of 15650 BH-BH, 1767 NS-NS and 769 BH-NS binaries. Thus, the lower metallicity used in model B causes an increase of the number of BHs that are formed and of their mean mass as well.

The average total mass  $\bar{M}$  and symmetric mass ratio  $\bar{\eta}$  are:

for model A

$$\begin{aligned} \bar{M} &= 15.41 M_{\odot} & \bar{\eta} &= 0.248 & \text{for BH-BH} \\ \bar{M} &= 2.43 M_{\odot} & \bar{\eta} &= 0.248 & \text{for NS-NS} \\ \bar{M} &= 9.94 M_{\odot} & \bar{\eta} &= 0.150 & \text{for BH-NS} \end{aligned} \quad (1)$$

for model B

$$\begin{aligned} \bar{M} &= 30.66 M_{\odot} & \bar{\eta} &= 0.246 & \text{for BH-BH} \\ \bar{M} &= 2.50 M_{\odot} & \bar{\eta} &= 0.249 & \text{for NS-NS} \\ \bar{M} &= 11.72 M_{\odot} & \bar{\eta} &= 0.117 & \text{for BH-NS} \end{aligned} \quad (2)$$

The procedure we adopt to compute the detection rates from the population synthesis statistics is the following.

Starting from the star formation rate density at a given redshift,  $\dot{\rho}_{\star}(z)$  (in units of  $M_{\odot} \text{ yr}^{-1} \text{ Mpc}^{-3}$ ), we derive the binary progenitors birth rate per comoving volume (in units of  $\text{yr}^{-1} \text{ Mpc}^{-3}$ ) as,

$$\frac{dR}{dt dV}(z) = A \times \dot{\rho}_{\star}(z) \quad (3)$$

where

$$A = \frac{f_{\text{bin}} \times f_{\text{sim}}}{2 \langle m_{\star} \rangle}, \quad (4)$$

$f_{\text{bin}}$  is the binarity fraction,  $\langle m_{\star} \rangle$  is the average stellar mass and  $f_{\text{sim}}$  is the fraction of binaries simulated by the population synthesis code. The latter quantity accounts for the fact that the range of progenitor masses used in the simulation is different from the range of validity of the adopted IMF. The factors  $f_{\text{sim}}$  and  $\langle m_{\star} \rangle$  depend on the adopted stellar Initial Mass Function (IMF),  $\Phi(m)$ , as

$$f_{\text{sim}} = \frac{\int_8^{100} dm \Phi(m)}{\int_{0.1}^{100} dm \Phi(m)}, \quad (5)$$

$$\langle m_{\star} \rangle = \frac{\int_{0.1}^{100} dm m \Phi(m)}{\int_{0.1}^{100} dm \Phi(m)}. \quad (6)$$

In [23] the authors set  $f_{\text{bin}} = 2/3$  and initialize the stellar progenitors in the mass range  $[5 - 150] M_{\odot}$  according to a Kroupa IMF.

We extract from the simulated sample of  $N_{\text{tot}}$  binaries, those systems with total mass  $\in (M, M+dM)$ , symmetric mass ratio  $\in (\eta, \eta+d\eta)$ , and delay time  $\in (t_d, t_d+dt_d)$ , which form BH-BH, NS-NS, and BH-NS systems; the delay time is defined as the time interval between the formation of the binary progenitor system and its coalescence. Their number is  $N_i(M, \eta, t_d)$ , where  $i$  refers to BH-BH, NS-NS, BH-NS systems.

The number of binaries coalescing at redshift  $z_c$ , with total mass  $M$  and symmetric mass ratio  $\eta$ , per unit of  $M$ ,  $\eta$  and comoving volume is  $(\text{Mpc}^{-3} \text{ yr}^{-1} M_{\odot}^{-1} \eta^{-1})$ :

$$\dot{r}_{\text{coal}}(M, \eta, z_c) = \int \frac{A \times \dot{\rho}_{\star}(z_f) N_i(M, \eta, t_d)}{1 + z_f N_{\text{tot}}} dt_d; \quad (7)$$

the redshifts of progenitor binary formation,  $z_f$ , and of binary coalescence,  $z_c$ , are related by the delay time as follows

$$t_d = \int_{z_c}^{z_f} \left| \frac{dt}{dz} \right| dz, \quad (8)$$

and

$$\left| \frac{dt}{dz} \right| = \frac{1}{H_0(1+z) \sqrt{\Omega_m(1+z)^3 + (1-\Omega_m)}}. \quad (9)$$

In this work we assume  $H_0 = 73 \text{ km}^{-1} \text{ Mpc}^{-1}$  and  $\Omega_m = 0.24$ , consistently with the choice done in [26] to derive our adopted cosmic star formation history, which reproduces the observational data available at  $z < 8$ [27].

The coalescence rate density  $\dot{\rho}_c(z_c)$  ( $\text{Mpc}^{-3} \text{ yr}^{-1}$ ), i.e. the number of compact binaries coalescing at redshift  $z_c$ , per unit time and unit comoving volume, is

$$\begin{aligned} \dot{\rho}_c(z_c) &= \iint \dot{r}_{\text{coal}}(M, \eta, z_c) dM d\eta \\ &= A \int dM \int d\eta \int \frac{\dot{\rho}_*(z_f) N_i(M, \eta, t_d)}{1+z_f} \frac{1}{N_{\text{tot}}} dt_d. \end{aligned} \quad (10)$$

In Fig. 1 we plot  $\dot{\rho}_c$  as a function of redshift for model

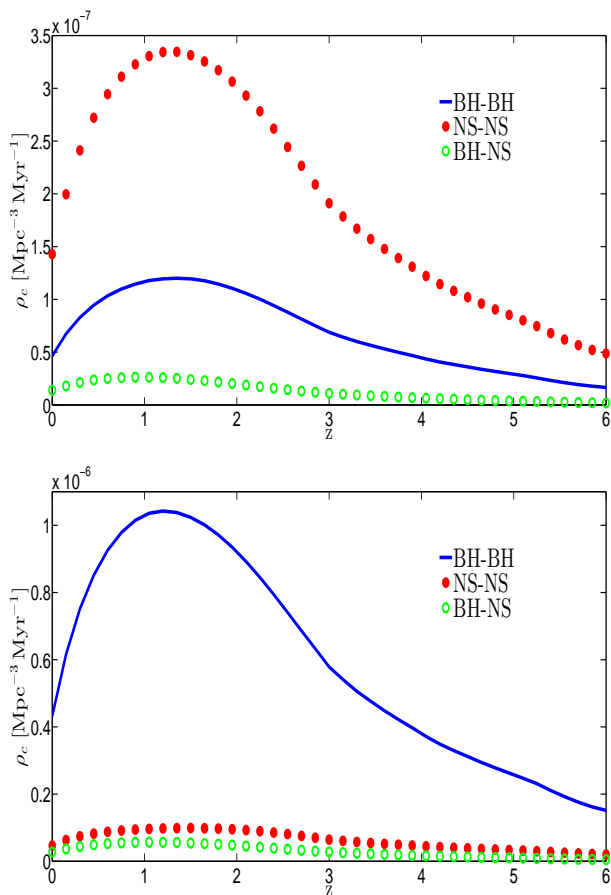


FIG. 1: (color online) The coalescence rate density computed with Eq. (10), is plotted versus redshift, respectively for BH-BH, NS-NS and BH-NS binaries, for model A and B.

A (upper panel) and model B (lower panel). We define the value  $\dot{\rho}_c^{\text{local}} = \dot{\rho}_c(z_c = 0)$  as the “local merger rate per unit comoving volume”. For model A we find

$$\begin{aligned} \dot{\rho}_c^{\text{local}} &= 4.64 \times 10^{-2} \text{ Mpc}^{-3} \times \text{Myr}^{-1} \quad (\text{BH-BH})(11) \\ \dot{\rho}_c^{\text{local}} &= 1.43 \times 10^{-1} \text{ Mpc}^{-3} \times \text{Myr}^{-1} \quad (\text{NS-NS}) \\ \dot{\rho}_c^{\text{local}} &= 1.40 \times 10^{-2} \text{ Mpc}^{-3} \times \text{Myr}^{-1} \quad (\text{BH-NS}). \end{aligned}$$

and for model B

$$\begin{aligned} \dot{\rho}_c^{\text{local}} &= 4.32 \times 10^{-1} \text{ Mpc}^{-3} \times \text{Myr}^{-1} \quad (\text{BH-BH})(12) \\ \dot{\rho}_c^{\text{local}} &= 4.69 \times 10^{-2} \text{ Mpc}^{-3} \times \text{Myr}^{-1} \quad (\text{NS-NS}) \\ \dot{\rho}_c^{\text{local}} &= 2.73 \times 10^{-2} \text{ Mpc}^{-3} \times \text{Myr}^{-1} \quad (\text{BH-NS}). \end{aligned}$$

To compute the detection rate, we sum over the sources which are within a given interferometer reach. Assuming that the signals are extracted from noise using the standard matched filtering technique, the Signal to Noise Ratio (SNR), averaged over sky positions and angles is [24]:

$$\langle \text{SNR} \rangle^2 = \frac{3}{2} \left\{ \frac{2}{5} \frac{(1+z)^2}{\pi^2 d_L(z)^2} \int_0^\infty df \frac{1}{f^2 S_h(f)} \frac{dE_e}{df_e} [(1+z)f] \right\}, \quad (13)$$

where  $f$  is the observed frequency, related to the source emission frequency  $f_e$  by

$$f = \frac{f_e}{1+z}, \quad (14)$$

$dE_e/df_e$  is the source energy spectrum, and  $S_h$  is the detector noise spectral density. For BH-BH systems we shall use the most recent hybrid waveforms produced by numerical relativity groups [28]. These describe the full inspiral-merger-ringdown phases of coalescence, accounting also for non-precessing spins. However, since the simulated populations we use do not include spins, we shall assume that all BH-BH systems have zero spin. For NS-NS and BH-NS binaries we use the chirp waveform, truncated to the ISCO. Moreover we will consider various noise curves of advanced detectors, namely Advanced LIGO (ALIGO) in four of its planned configurations [29]<sup>5</sup>, namely zero detuning high laser power (ALIGO1), optimized for 30-30 solar mass bh binary (ALIGO2), no signal recycling mirror (ALIGO3), and optimized for NS-NS binaries (ALIGO4), Advanced Virgo<sup>6</sup>(AVirgo), and ET<sup>7</sup> in three different configurations namely ET\_B, ET\_C and ET\_D.

We define  $z_{\text{max}}(M, \eta)$  as the maximum redshift at which a system with assigned  $(M, \eta)$  is detectable with  $\text{SNR}=8$ , averaging over position and orientation;  $z_{\text{max}}(M, \eta)$  is obtained by inverting Eq. (13).  $D_{\text{max}}(M, \eta)$  is the corresponding luminosity distance.

Moreover, we define  $z_h(M, \eta)$  and  $D_h(M, \eta)$ , as the horizon redshift and horizon distance, computed as before, but assuming optimal orientation.

The detection rate per unit total mass  $M$  and mass ratio  $\eta$ ,  $N_{M, \eta}$ , expressed in units [ $\text{yr}^{-1} \text{ M}_\odot^{-1} \eta^{-1}$ ], is found by integrating the function  $\dot{r}_{\text{coal}}(M, \eta, z_c)$  up to  $z_{\text{max}}(M, \eta)$ , as follows:

<sup>5</sup> see LIGO document LIGO-T0900288-v3

<sup>6</sup> [www.cascina.virgo.infn.it/~advirgo/docs/Adv\\_refsens\\_100512.txt](http://www.cascina.virgo.infn.it/~advirgo/docs/Adv_refsens_100512.txt)

<sup>7</sup> <http://www.et-gw.eu/etsensitivities>

No Approximation detection rates $N_{\text{det}}$ [ $\text{yr}^{-1}$ ]						
detector	BH-BH		NS-NS		BH-NS	
	model A	model B	model A	model B	model A	model B
AVirgo	73	$5.67 \cdot 10^3$	2.3	0.82	3.7	6.61
ALIGO1	203	$1.52 \cdot 10^4$	6.0	2.10	9.2	17.8
ALIGO2	134	$1.07 \cdot 10^4$	3.9	1.35	6.2	12.0
ALIGO3	105	$8.34 \cdot 10^3$	3.1	1.08	5.0	9.60
ALIGO4	254	$1.84 \cdot 10^4$	7.6	2.66	11.8	22.0
ET_B	$1.80 \cdot 10^5$	$1.56 \cdot 10^6$	$2.65 \cdot 10^4$	$8.01 \cdot 10^3$	$1.79 \cdot 10^4$	$3.62 \cdot 10^4$
ET_C	$1.84 \cdot 10^5$	$1.59 \cdot 10^6$	$4.48 \cdot 10^4$	$1.35 \cdot 10^4$	$2.47 \cdot 10^4$	$5.39 \cdot 10^4$
ET_D	$1.81 \cdot 10^5$	$1.57 \cdot 10^6$	$2.64 \cdot 10^4$	$7.95 \cdot 10^3$	$1.87 \cdot 10^4$	$3.86 \cdot 10^4$

TABLE I: Detection rates computed from Eq. (17), for the simulated populations of BH-BH, NS-NS and BH-NS (model A and B) and various detector sensitivities (first column) (see text).

$$N_{M,\eta}(M, \eta) = \int_0^{z_{\text{max}}(M,\eta)} \dot{r}_{\text{coal}}(M, \eta, z_c) \frac{dV}{dz_c} dz_c, \quad (15)$$

where the function

$$\frac{dV}{dz} = 4\pi c \frac{d_L(z)^2}{1+z} \left| \frac{dt}{dz} \right| \quad (16)$$

is the comoving volume element and  $d_L(z)$  is the luminosity distance. It has to be noted that  $N_{M,\eta}$  depends on  $M$  and  $\eta$ , not only through the coalescence rate  $\dot{r}_{\text{coal}}$ , but also through the integration limit. This means that, for each system (i.e. for each value of  $M$  and  $\eta$ ), the coalescence rate is integrated up to a different distance.

The integrated detection rate, i.e. the final output of our procedure, in units [ $\text{yr}^{-1}$ ] is:

$$\begin{aligned} N_{\text{det}} &= \int dM \int d\eta N_{M,\eta}(M, \eta) d\eta \\ &= \int dM \int d\eta \int_0^{z_{\text{max}}(M,\eta)} \dot{r}_{\text{coal}}(M, \eta, z_c) \frac{dV}{dz_c} dz_c. \end{aligned} \quad (17)$$

In the following we will refer to the results obtained with this procedure as the “no-approx” rates.

In Table I, we show the detection rates obtained for the three considered families of compact binaries, using model A and B. The uncertainty in these results, due to numerical integration, is of a few percent.

The data show that, for model A and B, the highest rates are attained by BH-BH systems, both for advanced and for third generation detectors.

As already noted in [20], where detection rates were computed only for advanced detectors, including metallicity effects in stellar evolution results in a much higher detection chance for BH-BH and BH-NS coalescing binaries. This is because in model B the number of these systems is larger than in model A, and the average mass of systems including BHs is higher (see Eqns. (1) and (2) and the text above).

Horizon distances $\bar{D}_h$ [Mpc]						
detector	model A			model B		
	BH-BH	NS-NS	BH-NS	BH-BH	NS-NS	BH-NS
AVirgo	1980	371	959	4030	381	955
ALIGO1	2980	518	1390	6110	533	1390
ALIGO2	2520	445	1200	5210	458	1200
ALIGO3	2290	412	1100	4580	423	1100
ALIGO4	3260	562	1510	6770	578	1500

TABLE II: Horizon distances of advanced detectors (in Mpc), computed for the mean values of mass and mass ratio given in Eqns. (1) and (2), for the three families of binaries and for models A and B.

Finally, in Table II we give the values of the horizon distance,  $\bar{D}_h \equiv D_h(\bar{M}, \bar{\eta})$ , which corresponds to the mean values of mass and mass ratio given in Eqns. (1) and (2); this quantity will be useful in the following discussion.

### III. COMPARISON WITH OTHER PROCEDURES

Various approaches have been used in the literature to compute detection rates, starting from the coalescence rates produced by population synthesis simulations [9, 12–22]. A common feature of these approaches is that the detection rate is evaluated by multiplying the merger rate by a properly defined detection volume  $V_h$ , rather than using Eq. (17).

In [9] the authors adopt the following procedure. Assuming that all black holes have  $M = 10 M_\odot$  and all neutron stars have  $M = 1.4 M_\odot$ , they define the average horizon distance  $D_h$ , such that a binary system is detected with a  $SNR \geq 8$  by a given detector.

A detection volume is defined as the Euclidean volume

Approximation 1: detection rates [ $\text{yr}^{-1}$ ]												
detector	model A						model B					
	BH-BH		NS-NS		BH-NS		BH-BH		NS-NS		BH-NS	
	$N_{\text{det}}^1$	$N_{\text{det}}$	$N_{\text{det}}^1$	$N_{\text{det}}$	$N_{\text{det}}^1$	$N_{\text{det}}$	$N_{\text{det}}^1$	$N_{\text{det}}$	$N_{\text{det}}^1$	$N_{\text{det}}$	$N_{\text{det}}^1$	$N_{\text{det}}$
AVirgo	79	73	2.4	2.3	3.8	3.7	$3.98 \cdot 10^3$	$5.67 \cdot 10^3$	0.78	0.82	7.86	6.61
ALIGO1	210	203	6.2	6.0	9.3	9.2	$1.07 \cdot 10^4$	$1.52 \cdot 10^4$	2.01	2.10	21.0	17.8
ALIGO2	140	134	4.0	3.9	6.5	6.2	$7.17 \cdot 10^3$	$1.07 \cdot 10^4$	1.30	1.35	14.1	12.0
ALIGO3	107	105	3.2	3.1	5.3	5.0	$5.36 \cdot 10^3$	$8.34 \cdot 10^3$	1.04	1.08	11.3	9.60
ALIGO4	260	254	7.9	7.6	12.3	11.8	$1.36 \cdot 10^4$	$1.84 \cdot 10^4$	2.55	2.66	25.2	22.0

TABLE III: The detection rate  $N_{\text{det}}^1$ , evaluated from Eq. (21) (Approx 1) for model A and B.  $N_{\text{det}}^1$  for BH-BH systems (column 2), is compared to the no-approx rates,  $N_{\text{det}}$ , computed from Eq. (17) (column 3). The additional columns refer to the same quantities evaluated for NS-NS and BH-NS binaries.

within  $D_h$ :

$$V_h = \frac{4}{3} \pi \left( \frac{D_h}{\text{Mpc}} \right)^3. \quad (18)$$

The detection rate is then computed by multiplying the Galactic coalescence rate,  $\dot{\rho}_c^{\text{gal}}$  expressed in units  $\text{Myr}^{-1} \text{MWE}G^{-1}$  (Milky Way Equivalent Galaxy), by the number of MWEs inside  $V_h$ ,  $G(D_h)$ ,

$$N_{\text{det}} = \dot{\rho}_c^{\text{gal}} \times G(D_h), \quad (19)$$

where

$$G(D_h) = V_h \times (0.0116) \times \frac{1}{2.26^3}, \quad (20)$$

The numerical factor 0.0116 is an estimate of the local number density of MWEs in units  $\text{Mpc}^{-3}$  obtained in [30]; the factor  $1/2.26^3$  is needed to average over sky position and orientation. This factor and the distance  $D_h$  in Eq. (18), in ref. [9] are computed neglecting the effect of redshift (see their footnote 90).

The Galactic coalescence rate,  $\dot{\rho}_c^{\text{Gal}}$  can be estimated following two different procedures, i.e. by using a constant Galactic star formation rate [31, 32], or by normalizing the number of binaries produced by a population synthesis code to the observed Galactic supernova rate [11, 21]. Using the former procedure, in [23] they find

- $\dot{\rho}_c^{\text{Gal}} = 8.2 \text{ MWE}G^{-1} \times \text{Myr}^{-1}$  for BH-BH,
- $\dot{\rho}_c^{\text{Gal}} = 23.5 \text{ MWE}G^{-1} \times \text{Myr}^{-1}$  for NS-NS,
- $\dot{\rho}_c^{\text{Gal}} = 1.6 \text{ MWE}G^{-1} \times \text{Myr}^{-1}$  for BH-NS.

for model A and

- $\dot{\rho}_c^{\text{Gal}} = 73.3 \text{ MWE}G^{-1} \times \text{Myr}^{-1}$  for BH-BH,
- $\dot{\rho}_c^{\text{Gal}} = 8.1 \text{ MWE}G^{-1} \times \text{Myr}^{-1}$  for NS-NS,
- $\dot{\rho}_c^{\text{Gal}} = 3.4 \text{ MWE}G^{-1} \times \text{Myr}^{-1}$  for BH-NS.

for model B. If the detection rate is estimated using the local coalescence rate per unit volume,  $\dot{\rho}_c^{\text{local}}$ , in units  $\text{Mpc}^{-3} \times \text{Myr}^{-1}$ , Eq. (19) reads

$$N_{\text{det}} = \dot{\rho}_c^{\text{local}} \times V_h \times \frac{1}{2.26^3}. \quad (21)$$

It should be noted that the ratio between the local and the Galactic rates depends on the adopted cosmic star formation history model, on the Galactic star formation rate, as well as on the statistical properties of the binary population (delay time distribution). In [9] a constant value of  $\dot{\rho}_c^{\text{local}}/\dot{\rho}_c^{\text{gal}} = 0.0116$ , has been adopted for all compact binaries considered in their study. In summary, the approximations done in [9] to estimate the detection rates predicted by different binary populations and different detectors are:

1. Approx 1: use of a single horizon distance  $D_h$  for all systems of a given binary population, corresponding to the mean values of mass and mass ratio.
2. Approx 2: evaluation of the detection rate by multiplying the local value of the coalescence rate density,  $\dot{\rho}_c(z=0)$ , by the Euclidean volume, within the horizon distance  $D_h$ , as in Eqns. (19) or (21).
3. Approx 3: evaluation of the horizon distance neglecting the redshift effects included in Eqns. (13) and (14).

In what follows, we investigate the effects of these approximations; since in [9] they are used all together, we will show the consequences of applying approximation 1, 1+2 and 1+2+3.

### A. Approximation 1

Approximation 1 consists in using the same horizon distance for all systems of a binary population, regardless of their individual total mass and symmetric mass ratio. To evaluate the effect of this approximation, we use the

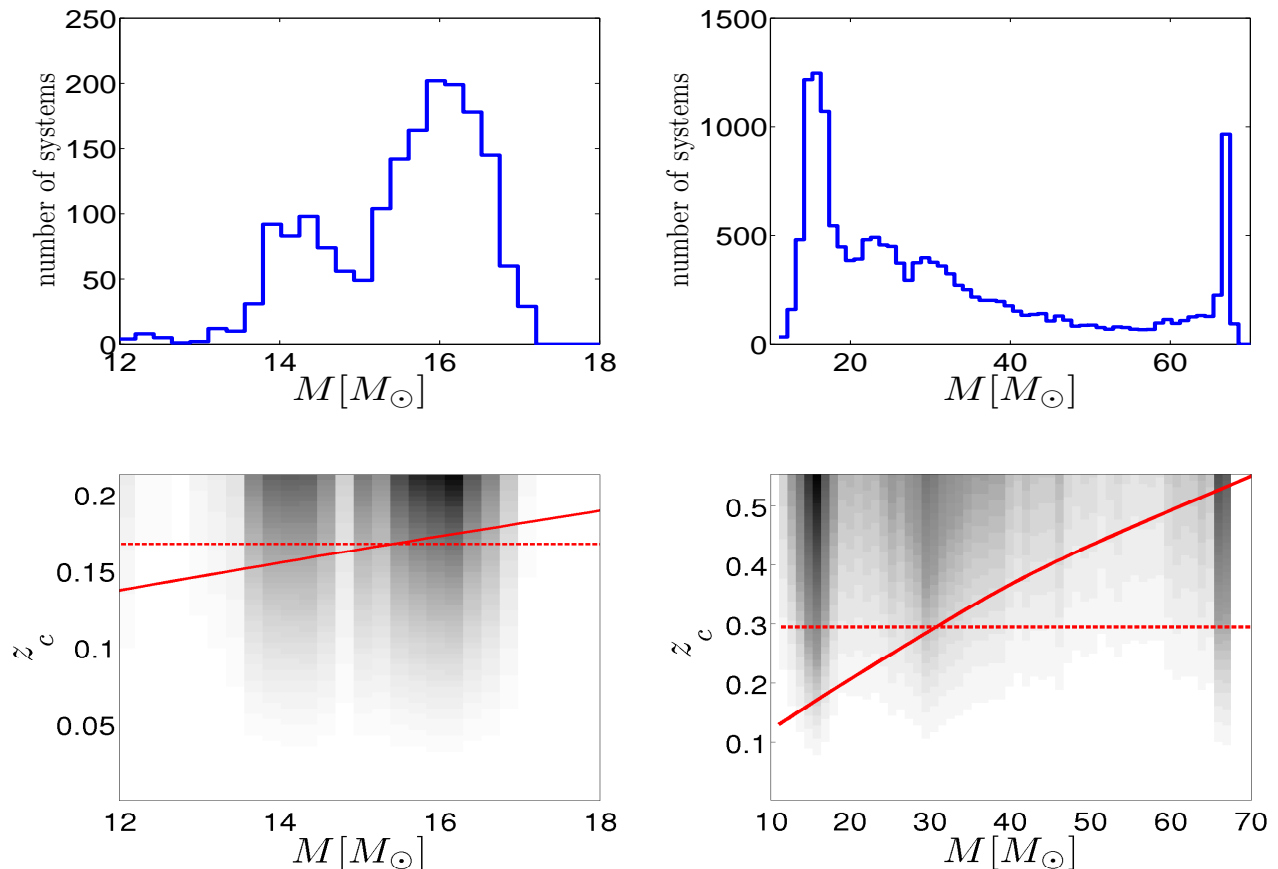


FIG. 2: The total mass distribution for BH-BH systems for model A (left) and B (right) is plotted in the upper panels. In the lower panels we plot the integrand of Eq. (22) as a function of  $M$  and redshift  $z_c$ , using a gray scale proportional to its value. The dashed line corresponds to  $z_{\max}(\bar{M}, \bar{\eta})$ , the solid line corresponds to the redshift up to which the system with a given total mass and  $\eta = \bar{\eta}$  would be detected with an average SNR of 8.

values of  $\bar{D}_h$  given in Table II, which correspond to the average values of  $M$  and  $\eta$  given in Eqns. (1) and (2). We then compute the detection rate  $N_{\text{det}}^1$ , by integrating Eq. (17) up to the redshift  $z_{\max}$

$$N_{\text{det}}^1 = \int dM \int_0^{z_{\max}} dz_c \int \dot{r}_{\text{coal}}(M, \eta, z_c) \frac{dV}{dz_c} d\eta, \quad (22)$$

where  $z_{\max} = z_{\max}(\bar{M}, \bar{\eta})$ . The results are shown in Table III. For model A, the difference between  $N_{\text{det}}^1$  and the no-approx rates  $N_{\text{det}}$  is of a few percent, for all binary populations, and  $N_{\text{det}}^1$  is always larger than  $N_{\text{det}}$ .

For model B, conversely, the difference between  $N_{\text{det}}^1$  and  $N_{\text{det}}$  ranges between -26% (ALIGO4) and -36% (ALIGO3) for BH-BH, and between +13% (ALIGO4) and +19% (AVirgo) for BH-NS. For NS-NS binaries the difference between  $N_{\text{det}}^1$  and  $N_{\text{det}}$  is, as for model A, of a few percent for all interferometers. Moreover, for BH-BH and NS-NS families,  $N_{\text{det}}^1$  is systematically smaller than  $N_{\text{det}}$ , while it is always larger for BH-NS.

These data show that the effect of Approx 1 depends on the model and on the kind of binary population. To

clarify this dependence, which will affect also the results obtained with Approx 2 and 3, in the upper panel of Fig. 2 we plot, as an example, the total mass distribution for BH-BH systems for model A (left) and B (right). In the lower panels we plot the function

$$\int \dot{r}_{\text{coal}}(M, \eta, z_c) \frac{dV}{dz_c} d\eta, \quad (23)$$

which appear in Eq. (22), as a function of  $M$  and of the redshift  $z_c$ , using a gray scale proportional to its value. In these panels, the horizontal dashed line corresponds to  $z_{\max}(\bar{M}, \bar{\eta})$ , whereas the solid line represent the function  $z_{\max}(M, \bar{\eta})$ , i.e. the redshift up to which the system with total mass  $M$  and symmetric mass ratio  $\bar{\eta}$  would be detected with an average SNR of 8. When the function (23) is integrated up to  $\bar{z}_h$  to compute the rate as in Eq. (22), the contribution of masses lower than the crossing point between the two lines is overestimated, whereas that of masses above that point is underestimated, with respect to their contribution in Eq. (17).

From Figure 2, we see that for model A, the two contributions nearly balance, whereas for model B, which

Approx 1+2: detection rates [ $\text{yr}^{-1}$ ]												
detector	model A						model B					
	BH-BH		NS-NS		BH-NS		BH-BH		NS-NS		BH-NS	
	$N_{\text{det}}^{12}$	$N_{\text{det}}$	$N_{\text{det}}^{12}$	$N_{\text{det}}$	$N_{\text{det}}^{12}$	$N_{\text{det}}$	$N_{\text{det}}^{12}$	$N_{\text{det}}$	$N_{\text{det}}^{12}$	$N_{\text{det}}$	$N_{\text{det}}^{12}$	$N_{\text{det}}$
AVirgo	91	73	2.7	2.3	4.6	3.7	$5.62 \cdot 10^3$	$5.67 \cdot 10^3$	0.94	0.82	9.20	6.61
ALIGO1	273	203	6.9	6.0	12.1	9.2	$1.73 \cdot 10^4$	$1.52 \cdot 10^4$	2.46	2.10	24.7	17.8
ALIGO2	173	134	4.4	3.9	7.9	6.2	$1.09 \cdot 10^4$	$1.07 \cdot 10^4$	1.56	1.35	16.4	12.0
ALIGO3	134	105	3.5	3.1	6.3	5.0	$8.09 \cdot 10^3$	$8.34 \cdot 10^3$	1.25	1.08	13.0	9.60
ALIGO4	347	254	8.8	7.6	15.7	11.8	$2.30 \cdot 10^4$	$1.84 \cdot 10^4$	3.12	2.66	31.5	22.0

TABLE IV: The detection rate  $N_{\text{det}}^{12}$ , evaluated from Eq. (21) using Approx 1+2, for model A and B.  $N_{\text{det}}^{12}$  for BH-BH systems (column 2), is compared to the no-approx rates,  $N_{\text{det}}$ , computed from Eq. (17) (column 3). The additional columns refer to the same quantities evaluated for NS-NS and BH-NS binaries.

Horizon distances [Mpc]												
detector	model A						model B					
	BH-BH		NS-NS		BH-NS		BH-BH		NS-NS		BH-NS	
	$\bar{D}_h^3$	$\bar{D}_h$	$\bar{D}_h^3$	$\bar{D}_h$	$\bar{D}_h^3$	$\bar{D}_h$	$\bar{D}_h^3$	$\bar{D}_h$	$\bar{D}_h^3$	$\bar{D}_h$	$\bar{D}_h^3$	$\bar{D}_h$
AVirgo	1540	1980	347	371	830	959	2650	4030	356	381	829	955
ALIGO1	2120	2980	474	518	1140	1390	3650	6110	486	533	1140	1390
ALIGO2	1860	2520	412	445	1000	1200	3200	5210	422	458	1000	1200
ALIGO3	1720	2290	383	412	931	1100	2960	4580	392	423	934	1100
ALIGO4	2280	3260	511	562	1230	1510	3920	6770	524	578	1230	1500

TABLE V: Average horizon distances (in Mpc) for the three families of binaries and for models A and B.  $\bar{D}_h^3$  is computed neglecting redshift contributions, whereas these are included in  $\bar{D}_h$ . Both quantities are evaluated using the mean values  $\bar{M}$  and  $\bar{\eta}$  given in Eqns. (1) and (2).

has a bimodal mass distribution, the high mass contribution, which is relevant, is neglected. This explains why, for the BH-BH population of model B,  $N_{\text{det}}^{12}$  is systematically lower than  $N_{\text{det}}$ . A similar explanation holds for the BH-NS population of model B, for which the low mass contributions is larger than the high mass one. Thus, the rate estimated using Approx 1 can either be larger or smaller than  $N_{\text{det}}$  by a different amount, depending on shape of the mass distribution. It has to be noted that the effect of this approximation is not related to the detector sensitivity because, for example, for model B the largest effect is for ALIGO3, which does not have the largest horizon distance (see Table II).

## B. Approximation 1+2

Approximation 2 assumes that the coalescence rate  $\dot{\rho}_c$  is constant through the whole detection volume  $V_h$ , and equal to the value at  $z = 0$  (Eqns. (19) or (21)). As a consequence, the dependence of the coalescence rate on redshift is completely neglected.

In addition, the detection rate is obtained by multiplying  $\dot{\rho}_c^{\text{local}} = \dot{\rho}_c(z = 0)$  by the Euclidean volume  $V_h$  (Eq. (18)) within  $D_{\text{max}}(\bar{M}, \bar{\eta})$ .

To assess the bias introduced using these approximations, we compute the detection rates,  $N_{\text{det}}^{12}$ , as:

$$N_{\text{det}}^{12} = \frac{4}{3}\pi D_{\text{max}}(\bar{M}, \bar{\eta})^3 \times \rho_c^{\text{local}} \quad (24)$$

The results are given in Table IV, where these are compared to the detection rates  $N_{\text{det}}$  computed in section II with no approximation.

Let us consider model A first. The values of  $N_{\text{det}}^{12}$  are always larger than those of  $N_{\text{det}}$ , i.e. Approx 1+2 overestimates the rates. The most significant differences are for BH-BH, and vary from +24% (AVirgo) to +37% (ALIGO4); for NS-NS they vary from +13% (ALIGO2,ALIGO3) to +17% (AVirgo) and for BH-NS from +24% (AVirgo) to +33% (ALIGO4). Since, as discussed above, for model A Approx 1 does not introduce a significant bias in the estimated rates, it is clear that the differences are due mainly to Approx 2 alone.

These can be traced back to the contribution of the two assumptions: the first is that  $\dot{\rho}_c$  is assumed to be constant and equal to the  $z = 0$  value, while it is clear from Fig. 1, that this is not the case. This assumption alone would lead to an underestimate of the rates for all families because, in the range of interest for  $z$ , the function  $\dot{\rho}_c(z)$  is always larger than the local value. Conversely, the second

Approx 1+2+3: detection rates [yr <sup>-1</sup> ]												
detector	model A						model B					
	BH-BH		NS-NS		BH-NS		BH-BH		NS-NS		BH-NS	
	$N_{\text{det}}^{123}$	$N_{\text{det}}$	$N_{\text{det}}^{123}$	$N_{\text{det}}$	$N_{\text{det}}^{123}$	$N_{\text{det}}$	$N_{\text{det}}^{123}$	$N_{\text{det}}$	$N_{\text{det}}^{123}$	$N_{\text{det}}$	$N_{\text{det}}^{123}$	$N_{\text{det}}$
AVirgo	63.3	73	2.4	2.3	3.7	3.7	$3.0 \cdot 10^3$	$5.67 \cdot 10^3$	0.85	0.82	7.43	6.61
ALIGO1	166	203	6.1	6.0	9.0	9.2	$7.85 \cdot 10^3$	$1.52 \cdot 10^4$	2.15	2.10	18.4	17.8
ALIGO2	111	134	3.9	3.9	6.1	6.2	$5.31 \cdot 10^3$	$1.07 \cdot 10^4$	1.40	1.35	12.5	12.0
ALIGO3	88.9	105	3.2	3.1	4.9	5.0	$4.21 \cdot 10^3$	$8.34 \cdot 10^3$	1.12	1.08	10.1	9.60
ALIGO4	204	254	7.7	7.6	11.5	11.8	$9.76 \cdot 10^3$	$1.84 \cdot 10^4$	2.71	2.66	23.2	22.0

TABLE VI: The detection rates computed using Approx 1+2+3, i.e. neglecting the effect of redshift, and assuming that the merger rate is constant through the detection volume, and equal to its local value. The detection rates  $N_{\text{det}}$ , computed with the no-approx procedure (Eq. (17)) are given for comparison.

assumption, i.e. that the local coalescence rate is multiplied by the Euclidean volume, leads to an overestimate of the rates, because the Euclidean volume is larger than the cosmological one, and this effect is larger than the former, so that the combined result is an overestimate of the detection rates for all the three families.

For model B, the detection rates  $N_{\text{det}}^{12}$  given in Table IV, differ (in percentual) from the corresponding values of  $N_{\text{det}}$  as follows: for BH-BH from -3% (ALIGO3) to +25% (ALIGO4), for NS-NS from +15% (AVirgo) to +17% (ALIGO1,ALIGO4), for BH-NS from +35% (ALIGO3) to +43% (ALIGO4). By comparing  $N_{\text{det}}^{12}$  in table III with  $N_{\text{det}}^{12}$  in table IV we see that also in this case the effect of Approx 2 alone is to raise the rates obtained with Approx 1 alone. It should be noted that, contrary to the results of Approx 1, the effect of Approx 2 depends on the reach of the interferometer, and is larger for interferometers with higher sensitivity. This is particularly evident for model A, where the effects of Approx 1 are negligible, while those of Approx 1+2 increase going from AVirgo to ALIGO4, which has the highest sensitivity.

For model B the effect of Approx 1 is not negligible, so that the effect of Approx 1+2 varies between interferometers and binary families.

### C. Approximation 1+2+3

Approximation 3 does not include redshift contributions in the SNR evaluation. This will reflect in different values for  $D_{\text{h}}$  and  $D_{\text{max}}$  which we will denote as  $D_{\text{h}}^3$  and  $D_{\text{max}}^3$ . In Table V we compare the horizon distances  $\bar{D}_{\text{h}}$  given in Table II, and which include redshift contribution, to  $\bar{D}_{\text{h}}^3 \equiv D_{\text{h}}^3(\bar{M}, \bar{\eta})$ .

Horizon distances computed neglecting the redshift are smaller than those which include it, and this reflects into smaller detection rates, as can be seen by comparing the rates  $N_{\text{det}}^{12}$  in table IV for approx 1+2, with  $N_{\text{det}}^{123}$ , given in Table VI and computed for Approx 1+2+3. As expected, the difference is larger for interferometers with larger horizon distances.

Turning to the comparison between  $N_{\text{det}}^{123}$  and  $N_{\text{det}}$ , shown in Table VI, we see that the percentage differences for the three families of binaries range within: for model A, from -13% (AVirgo) to -18% (ALIGO1) for BH-BH, from 0 (ALIGO2) to +4% (AVirgo) for NS-NS, and from 0 (AVirgo) to -3% (ALIGO4) for BH-NS; for model B, from -47% (AVirgo) to -51% (ALIGO2) for BH-BH, from +2% (ALIGO1,ALIGO4) to +4% (AVirgo,ALIGO2,ALIGO3) for NS-NS, from +3% (ALIGO1) to +12% (AVirgo) for BH-NS.

Thus, it is clear that Approx 1+2+3, which has been used to estimate the detection rates of second generation detectors in [18–21], can result in an overestimate or underestimate of the rates depending on the details of the population and on the interferometer which is considered.

## IV. CONCLUDING REMARKS

In this paper we discuss the procedure to compute the detection rates for coalescing compact binaries, to be detected by the advanced detectors expected to be in operation in a few years. We quantify the effect of various approximations adopted in the literature to estimate these rates, and show that they introduce a bias which depends not only on the approximation which is used, but also on the statistical properties of the considered binary population (BH-BH, NS-NS, or BH-NS). These properties depend on the physical inputs introduced in the population synthesis codes used to generate the population, and these may vary significantly from one model to another. An example is shown in Figure 2, where the difference between the mass distribution of BH-BH binaries for model A, which assumes solar metallicity, and model B, based on subsolar metallicity, is apparent.

Thus, if we want to associate a detection rate to a given population of binaries, derived on the basis of some physical assumptions, we need to use the fully consistent procedure described in section II; indeed, the use of approximations as those described in section III, would not allow to disentangle the effects of the physical inputs



from those of the assumed approximations. Finally, we give an estimate of the detection rates for the Einstein Telescope, ET, using two population models obtained by the updated version of the *Startrack* code, which are publicly available. These rates have been obtained using the no approximation procedure, which is the only one applicable to ET, due to its high sensitivity.

## Acknowledgments

We would like to thank the *Startrack* collaboration, for making the results of *Startrack* available to the community on website <http://www.syntheticuniverse.org>.

- 
- [1] M. Punturo, M. Abernathy, F. Acernese, B. Allen, N. Andersson, K. Arun, F. Barone, B. Barr, M. Barsuglia, M. Beker, et al., *Classical and Quantum Gravity* **27**, 194002 (2010).
- [2] T. Regimbau, T. Dent, W. Del Pozzo, S. Giampanis, T. G. F. Li, C. Robinson, C. Van Den Broeck, D. Meacher, C. Rodriguez, B. S. Sathyaprakash, et al., *ArXiv e-prints* (2012), 1201.3563.
- [3] B. Sathyaprakash, M. Abernathy, F. Acernese, P. Ajith, B. Allen, P. Amaro-Seoane, N. Andersson, S. Aoudia, K. Arun, P. Astone, et al., eprint arXiv:1206.0331 (2012), 1206.0331.
- [4] B. S. Sathyaprakash, B. F. Schutz, and C. Van Den Broeck, *Classical and Quantum Gravity*, Volume 27, Issue 21, pp. 215006 (2010). **27**, 215006 (2010), 0906.4151.
- [5] S. R. Taylor and J. R. Gair, eprint arXiv:1204.6739 (2012), 1204.6739.
- [6] S. R. Taylor, J. R. Gair, and I. Mandel, *Phys. Rev. D* **85**, 023535 (2012), 1108.5161.
- [7] J. Abadie, B. P. Abbott, R. Abbott, M. Abernathy, T. Accadia, F. Acernese, C. Adams, R. Adhikari, P. Ajith, B. Allen, et al., *Phys. Rev. D* **83**, 122005 (2011), 1102.3781.
- [8] J. Abadie, B. P. Abbott, R. Abbott, T. D. Abbott, M. Abernathy, T. Accadia, F. Acernese, C. Adams, R. Adhikari, C. Affeldt, et al., *Phys. Rev. D* **85**, 022001 (2012), 1110.0208.
- [9] J. Abadie, B. P. Abbott, R. Abbott, M. Abernathy, T. Accadia, F. Acernese, C. Adams, R. Adhikari, P. Ajith, B. Allen, et al., *Classical and Quantum Gravity* **27**, 173001 (2010), 1003.2480.
- [10] J. R. Gair, I. Mandel, M. C. Miller, and M. Volonteri, *General Relativity and Gravitation* **43**, 485 (2011), 0907.5450.
- [11] S. Marassi, R. Schneider, G. Corvino, V. Ferrari, and S. P. Zwart, *Phys. Rev. D* **84**, 124037 (2011), 1111.6125.
- [12] I. Mandel and R. O’Shaughnessy, *Classical and Quantum Gravity* **27**, 114007 (2010), 0912.1074.
- [13] T. Bulik, K. Belczyński, and B. Rudak, *A&A* **415**, 407 (2004), arXiv:astro-ph/0307237.
- [14] T. Bulik, D. Gondek-Rosinska, and K. Belczynski, *Monthly Notices of the RAS* **352**, 1372 (2004), arXiv:astro-ph/0310544.
- [15] R. Voss and T. M. Tauris, *Monthly Notices of the RAS* **342**, 1169 (2003), arXiv:astro-ph/0303227.
- [16] R. O’Shaughnessy, V. Kalogera, and K. Belczynski, *Astrophys. J.* **716**, 615 (2010), 0908.3635.
- [17] R. O’Shaughnessy, K. Belczynski, and V. Kalogera, *Astrophys. J.* **675**, 566 (2008), 0706.4139.
- [18] R. O’Shaughnessy, C. Kim, V. Kalogera, and K. Belczynski, *Astrophys. J.* **672**, 479 (2008), arXiv:astro-ph/0610076.
- [19] K. Belczynski, T. Bulik, and C. Baily, *Astrophysical Journal, Letters* **742**, L2 (2011), 1107.4106.
- [20] K. Belczynski, M. Dominik, T. Bulik, R. O’Shaughnessy, C. Fryer, and D. E. Holz, *Astrophysical Journal, Letters* **715**, L138 (2010), 1004.0386.
- [21] K. Belczynski, R. E. Taam, V. Kalogera, F. A. Rasio, and T. Bulik, *Astrophys. J.* **662**, 504 (2007), arXiv:astro-ph/0612032.
- [22] R. O’Shaughnessy, C. Kim, T. Fragos, V. Kalogera, and K. Belczynski, *Astrophys. J.* **633**, 1076 (2005), arXiv:astro-ph/0504479.
- [23] M. Dominik, K. Belczynski, C. Fryer, D. Holz, E. Berti, T. Bulik, I. Mandel, and R. O’Shaughnessy, *ArXiv e-prints* (2012), 1202.4901.
- [24] É. É. Flanagan and S. A. Hughes, *Phys. Rev. D* **57**, 4535 (1998), arXiv:gr-qc/9701039.
- [25] R. Schneider, V. Ferrari, S. Matarrese, and S. F. Portegies Zwart, *Monthly Notices of the RAS* **324**, 797 (2001), arXiv:astro-ph/0002055.
- [26] L. Tornatore, A. Ferrara, and R. Schneider, *Monthly Notices of the RAS* **382**, 945 (2007), 0707.1433.
- [27] R. J. Bouwens, G. D. Illingworth, P. A. Oesch, M. Stiavelli, P. van Dokkum, M. Trenti, D. Magee, I. Labbé, M. Franx, C. M. Carollo, et al., *Astrophysical Journal, Letters* **709**, L133 (2010), 0909.1803.
- [28] P. Ajith, M. Hannam, S. Husa, Y. Chen, B. Brügmann, N. Dorband, D. Müller, F. Ohme, D. Pollney, C. Reisswig, et al., *Physical Review Letters* **106**, 241101 (2011), 0909.2867.
- [29] G. M. Harry and LIGO Scientific Collaboration, *Classical and Quantum Gravity* **27**, 084006 (2010).
- [30] R. K. Kopparapu, C. Hanna, V. Kalogera, R. O’Shaughnessy, G. González, P. R. Brady, and S. Fairhurst, *Astrophys. J.* **675**, 1459 (2008), 0706.1283.
- [31] G. Nelemans, L. R. Yungelson, and S. F. Portegies Zwart, *A&A* **375**, 890 (2001), arXiv:astro-ph/0105221.
- [32] R. O’Shaughnessy, V. Kalogera, and K. Belczynski, *The Astrophysical Journal* **667**, 1048 (2007).